Applied Thermal Engineering 37 (2012) 30–37

Contents lists available at SciVerse ScienceDirect

Applied Thermal Engineering

journal homepage: www.elsevier.com/locate/apthermeng

Pyroelectric waste heat energy harvesting using heat conduction

Felix Y. Lee, Ashcon Navid, Laurent Pilon*

Mechanical and Aerospace Engineering Department, Henry Samueli School of Engineering and Applied Science, University of California, Los Angeles, CA 90095, USA

ARTICLE INFO

Article history:
Received 21 September 2011
Accepted 20 December 2011
Available online 30 December 2011

Keywords:
Pyroelectric materials
Ferroelectric materials
Direct energy conversion
Heat conduction
Waste heat harvesting
Olsen cycle

ABSTRACT

Waste heat can be directly converted into electrical energy by performing the Olsen cycle on pyroelectric materials. The Olsen cycle consists of two isothermal and two isoelectric field processes in the displacement versus electric field diagram. This paper reports, for the first time, a procedure to implement the Olsen cycle by alternatively placing a pyroelectric material in thermal contact with a cold and a hot source. Poly(vinylidene fluoride–trifluroethylene) [P(VDF–TrFE)] copolymer thin films with 60/40 VDF/TrFE mole fraction were used. A maximum energy density of 155 J/L per cycle was achieved at 0.066 Hz between 25 and 110 °C and electric fields cycled between 200 and 350 kV/cm. This energy density was larger than that achieved by our previous prototypical device using oscillatory laminar convective heat transfer. However, it was lower than the energy density obtained in previous "dipping experiments" consisting of alternatively dipping the samples in cold and hot silicone oil baths. This was attributed to (1) the lower operating temperatures due to the slow thermal response achieved using heat conduction and (2) the smaller electric field spans imposed which was limited by the smaller dielectric strength of air. However, the proposed procedure can readily be implemented into devices.

1. Introduction

Large amounts of waste heat are released as a by-product of power, refrigeration, or heat pump cycles according to the second law of thermodynamics [1]. In 2009, over 55% of the energy consumed in the United States was lost as low temperature waste heat typically discharged to the environment [1]. Opportunities exist to recycle this free source of waste heat into usable energy [2]. For example, Stirling engines directly convert thermal energy into mechanical energy for heat pump, cryogenic refrigeration, and air liquefaction applications [3]. Organic Rankine cycles use refrigerants and hydrocarbons to harvest waste heat up to 200–300 °C [4,5]. However, their performance is limited by heat losses and they cannot function well below 80 °C. Moreover, direct energy conversion using thermoelectric devices have been studied intensively. They make use of the Seebeck effect to convert a steady-state temperature difference at the junction of two dissimilar metals or semiconductors into an electromagnetic force (emf) or electrical energy [6]. Alternatively, pyroelectric energy devices directly convert time-dependent temperature oscillations into electricity [5,7–26]. In practice, the generated energy can be harvested by delivering it to an external load or storage unit [23,26]. Pyroelectric energy conversion devices require thermal cycling of a pyroelectric element (PE) between a hot and a cold temperature source to produce electricity. Various modes of heat transfer can be used to create the desired temperature oscillations [16,21,22,27]. The present study investigates the use of heat conduction in pyroelectric energy conversion using commercial 60/40 mol% poly(vinylidene fluoride–trifluorethylene) [P(VDF–TrFE)] copolymer thin films.

2. Background

2.1. Pyroelectric materials

Pyroelectric materials possess a spontaneous polarization defined as the average electric dipole moment per unit volume in absence of an applied electric field [28]. A subclass of pyroelectric materials known as ferroelectric materials have the ability to switch the direction and magnitude of the spontaneous polarization by reversing the applied coercive electric field [29]. Note that all ferroelectric materials are pyroelectric and all pyroelectric materials are piezoelectric. However, the converse is not true.

Fig. 1 shows the unipolar hysteresis curves between electric displacement D and electric field E exhibited by ferroelectric materials at two different temperatures T_{cold} and T_{hot}. The curves travel in a counter-clockwise direction upon isothermal cycling of electric field applied across the sample. When a ferroelectric material is heated above its Curie temperature T_{Curie} it undergoes

* Corresponding author. Tel.: +1 310 206 5598; fax: +1 310 206 4830.
E-mail address: pilon@seas.ucla.edu (L. Pilon).
URL: http://www.seas.ucla.edu/~pilon

1359-4311/$ – see front matter © 2011 Elsevier Ltd. All rights reserved.
doi:10.1016/j.applthermaleng.2011.12.034

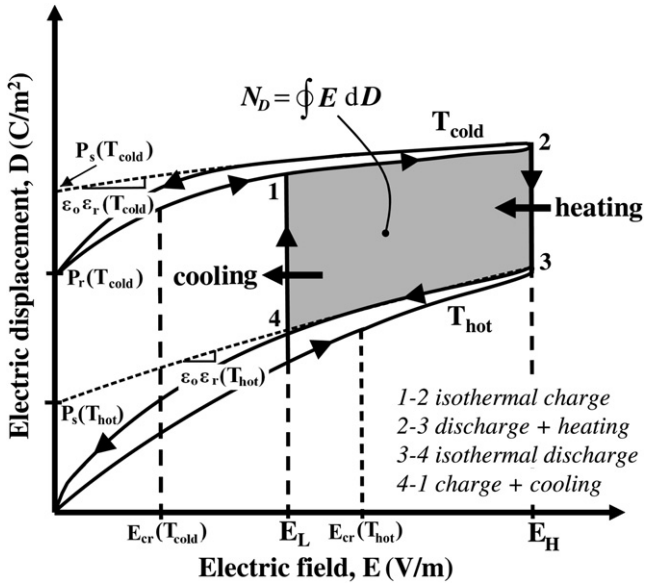

Fig. 1. Isothermal unipolar electric displacement versus electric field (D–E) hysteresis loops for a typical pyroelectric material at temperatures T_{hot} and T_{cold} along with the Olsen cycle. The electrical energy generated per cycle is represented by the area enclosed between 1–2–3–4.

a phase transition from ferroelectric to paraelectric. Then, the spontaneous polarization vanishes. The electric displacement D of the material at temperature T and electric field E is defined as [29,30]

$$D(E,T) = \varepsilon_0\varepsilon_r(T)E + P_s(T) \quad (1)$$

where ε_o is the vacuum permittivity ($=8.854\times10^{12}$ F/m), $\varepsilon_r(T)$ is the relative permittivity of the material, and E is the applied electric field. The saturation polarization denoted by $P_s(T)$ is estimated as the displacement in the linear fit of D versus E extrapolated at zero electric field. Copolymer P(VDF–TrFE) is a ferroelectric material whose Curie temperature can be varied by adjusting the VDF/TrFE ratio. Thermophysical and dielectric properties of 60/40 P(VDF–TrFE) for temperatures between 25 and 100 °C have been reported by Navid *et al.* [31].

2.2. Pyroelectric energy conversion

2.2.1. Olsen cycle

The Olsen cycle [7] is executed on pyroelectric films or slabs with metallic electrodes deposited on both sides. It consists of two isothermal and two isoelectric field processes [22]. Fig. 1 shows the Olsen cycle in the electric displacement versus electric field (D–E) diagram. The cycle starts when the PE is charged at T_{cold} by increasing the applied electric field from E_L to E_H (Process 1–2). Next, the PE is discharged by heating the element from T_{cold} to T_{hot} at constant electric field E_H (Process 2–3). The material is further discharged by reducing the electric field from E_H to E_L at constant temperature T_{hot} (Process 3–4). Finally, the PE is recharged by cooling the material from T_{hot} to T_{cold} at constant electric field E_L (Process 4–1). The enclosed area under the clockwise 1–2–3–4 loop in the D–E curve corresponds to the electric energy produced per unit volume of material per cycle denoted by N_D (in J/L/cycle) and given by [7]

$$N_D = \oint E\mathrm{d}D. \quad (2)$$

The corresponding power density generated by the pyroelectric element is given by

$$P_D = N_D f \quad (3)$$

where f is the cycle frequency. As the material approaches T_{Curie}, the isothermal D–E loops gradually become narrow and linear. As a result, the area bounded by the points 1–2–3–4 increases. Thus, it is desirable to heat the pyroelectric material above T_{Curie} in order to maximize the electrical energy generated. Similarly, increasing the electric field span $E_H - E_L$, without electric breakdown, results in larger N_D.

2.2.2. Leakage current

P(VDF–TrFE) is subject to leakage current particularly at high electric fields and/or high temperature [5,32–34]. Leakage current refers to the transport of charges accumulated at the surface of the pyroelectric element through its body [16]. In this process, energy is dissipated as Joule heating and in turn reduces the energy and power densities generated [22]. Several techniques can be used to reduce leakage current. First, the maximum operating temperature T_{hot} and maximum electric field E_H in the Olsen cycle can be reduced. In addition, increasing the frequency of the pyroelectric cycle can reduce leakage current by limiting the time during which the PE operates at E_H and T_{hot}. Furthermore, purifying pyroelectric materials may reduce leakage by eliminating defects in the film [5]. Finally, the PE can be poled prior to performing the Olsen cycle to increase its electrical resistance [31]. Maintaining a non-zero electric field ($E_L \simeq 200$ kV/cm) was recommended to keep the P(VDF–TrFE) films properly poled during the cooling Process 1–2 in the Olsen cycle [5,10,31,33].

2.2.3. Dipping experiments

A simple method for implementing the Olsen cycle is to successively dip the PE in hot and cold baths under specified electric fields [16]. The experimental setup and technique was described in Refs. [10,16]. The so-called "dipping experiments" are performed to assess the maximum amount of energy and power that can be generated under somehow idealized conditions without considering challenges associated with heat transfer limitations and devices assembly. Moreover, it facilitates the rapid screening for promising pyroelectric materials to be used in energy harvesting devices. Olsen *et al.* [10] performed the dipping experiments on 70–100 μm thick 60/40P(VDF–TrFE) films in 100 cSt silicone oil baths at $T_{cold} = 25$ °C and T_{hot} ranging from 100 to 120 °C. A constant low electric field $E_L = 200$ kV/cm was applied while the high electric field E_H varied between 200 and 600 kV/cm. A maximum output energy density of 900 J/L/cycle at $T_{hot} = 120$ °C and $E_H = 500$ kV/cm was reported at 0.125 Hz [10]. However, it is unclear whether the experimental results were averaged over multiple cycles and/or were repeatable. Navid *et al.* [16] extended the experimental investigation of pyroelectric conversion using the Olsen cycle for commercial, purified, and porous 60/40P(VDF–TrFE) films. Prior to performing the cycles, the 50 μm thick films were poled for 120 min under an electric field of 200 kV/cm at 95 °C to increase the film's electrical resistivity. The films were successively dipped in cold and hot 50 cSt silicone oil baths at 25 °C and 110 °C, respectively, under low and high electric fields $E_L = 200$ kV/cm and $E_H = 500$ kV/cm, respectively. The maximum energy density produced per cycle was 521 J/L, 426 J/L, and 188 J/L for commercial, purified, and porous films, respectively.

Moreover, Kandilian *et al.* [27] performed the Olsen cycle to assess the energy generating performance of 140 μm thick single crystal PMN-32PT capacitors [27]. The materials were alternatively dipped in cold and hot 200 cSt silicone oil baths, maintained at 80 °C and 130–170 °C, respectively. A maximum energy density of 100 J/L/cycle [27] was obtained under low and high electric fields $E_L = 2$ kV/cm and $E_H = 9$ kV/cm, respectively. Recently, McKinley

et al. [35] performed the same procedure on [001]-poled PZN-5.5PT single crystals and obtained a maximum energy density obtained of 150 J/L/cycle for temperatures between 100 and 190 °C and electric field between 0 and 12 kV/cm.

2.2.4. Forced convection devices

Several prototypical pyroelectric energy converters [7–9,11,33] implementing the Olsen cycle were designed and built in the 1980's. For example, Olsen *et al.* [7–11] assembled a regenerative and multistage device using 250 μm thick lead zirconate stanate tinanate (PZST) as the pyroelectric materials and silicone oil with viscosities of 50 and 200 cSt as the working fluids. The electric field was cycled between 4 and 28 kV/cm. The cold and hot source temperatures were 145 and 178 °C, respectively. A piston was used to vertically oscillate the working fluid back and forth between a cold and a hot source [11]. Temperature oscillations within the PE films were achieved by laminar forced convection between the silicone oil and the PE. A maximum power density of 33 W/L was obtained at 0.26 Hz. The maximum efficiency of 1.05% was achieved at 0.14 Hz, corresponding to 12% of the Carnot efficiency. Moreover, due to the high cost of PZST per Watt generated, Olsen *et al.* [33] built a device using inexpensive 30–70 μm thick 73/27 mol% P(VDF–TrFE) films. The maximum output energy density of this device was 30 J/L/cycle at 0.079 Hz, while operating at temperatures between 20 and 90 °C and electric fields between 230 and 530 kV/cm.

More recently, Nguyen *et al.* [22] assembled and operated a prototypical pyroelectric converter using 60/40P(VDF–TrFE). The experimental design was inspired by the device assembled by Olsen *et al.* [33] and informed by numerical simulations performed by Navid *et al.* [15]. The maximum energy density was 130 J/L/cycle at 0.061 Hz between 66.4 and 83 °C and 202 and 379 kV/cm. In addition, the maximum power density obtained was 10.7 W/L at 0.12 Hz between 67.3 and 81.4 °C and 202 and 379 kV/cm [22].

2.2.5. Nanoscale radiation

A pyroelectric material can reach its phase transition temperature rapidly during the Olsen cycle when heated by nanoscale radiation [21]. Fang *et al.* [21] performed numerical simulations of a pyroelectric converter harvesting nanoscale thermal radiation using 60/40P(VDF–TrFE) and 0.9PMN-PT. The simulations showed that an efficiency of 0.2% and an electrical power output of 0.84 mW/cm^2 was possible by using 60/40P(VDF–TrFE) with cold and hot sources at 273 and 388 K, respectively. For multilayer composite thin film 0.9PMN-PT, an efficiency of 1.35% and a power output of 6.5 mW/cm^2 was predicted for cold and hot plates at 283 and 383 K [21]. The simulated operating frequency was 1.2 Hz, more than ten times greater than that of actual devices employing laminar convective heat transfer [16,21,22]. Unfortunately, maintaining a nanoscale gap ($\sim$100 nm or less) between the PE and the hot or cold plates can be challenging. In the limiting case, the PE can be placed in thermal contact with the hot and cold sources. Then, heat is transferred by conduction. This presents the advantage of being inexpensive and easy to implement. However, the thermal response of the PE heated by heat conduction is expected to be slower than that obtained with other heat transfer modes. Indeed, conductive heat transfer is a diffusive process limited by thermal contact resistance between the PE and the cold or hot plates.

This paper reports experimental studies evaluating heat conduction as a way to heat and cool a pyroelectric element undergoing the Olsen cycle. These "stamping experiments" enable us to assess the effect of the heat transfer mode on the material performance. It is a proof of concept towards the design, assembly, and operation of a device. The results were compared with those previously reported for different heat transfer modes.

3. Experiments

3.1. Sample

Commercial 60/40P(VDF–TrFE) films were synthesized by the same method described in Ref. [31]. The PE used in the present study was 60.45 μm thick and approximately 2 cm in diameter. The cross-sectional area of the aluminum electrodes was 1 cm × 1 cm.

3.2. Experimental setup

Fig. 2 shows a schematic of the experimental setup. It consisted of a thermal and an electrical subsystem. The thermal system consisted of two 3 cm × 2.5 cm × 1.27 cm cold and hot aluminum blocks. They were used as the cold and hot sources maintained at the temperatures T_C and T_H, respectively. A 50 W Omega CS-10150 cartridge heater was embedded in the hot block and its temperature T_H was controlled thanks to an Omega CN-7823 proportional integral derivative (PID) temperature controller. The cold block was maintained at room temperature by free convection to the surrounding air at atmospheric pressure. A thermal conductive epoxy Omegabond-200 [36] layer with high electrical resistance and high thermal conductivity was applied on the top surfaces of both blocks. It electrically isolated the PE's electrodes from the metallic blocks while minimizing the thermal contact resistance. Its thermal conductivity was 1.384 W/m K and its electrical resistivity was on the order of 10^{15} Ω cm [36]. The PE sample was taped to the flat base of a wooden stamp. The wooden stamp allowed for convenient and safe handling of the film under various applied pressures. J-type thermocouples were embedded at the center of the hot and cold blocks. In addition, a J-type thermocouple was attached to the top of the film in such a way that it was in thermal contact but not in electrical contact with the electrodes. Since the film thickness was only tens of micrometers, the temperatures measured by the thermocouple was assumed to be the same across the film.

Fig. 3 shows the electrical subsystem used for performing the Olsen cycle. It consisted of a modified Sawyer-Tower circuit [30] to apply the required electric field and to measure charge Q collected on the PE electrodes. A resistive voltage divider was placed in parallel with the Sawyer-Tower bridge to control the electric field applied to the material. Voltage V_1 across the film capacitor C_1 was measured using a Burr–Brown DIFET electrometer (OPA128) to minimize discharge of the capacitor connected to an IOtech 3000 series data acquisition system (DAQ). The resistor R_L acted as a voltage divider to scale down the voltage across the resistor R_2 in order to match the maximum voltage input of 10 V of the DAQ. The electric field was applied by a computer generated function through the DAQ connected to a TREK 610E high voltage power supply. The magnitude of the film electric displacement D was defined as

$$D = \frac{Q}{A} = \frac{C_1 V_1}{A} \tag{4}$$

where $A = 1$ cm^2 is the film surface area. The magnitude of the electric field across the PE was calculated from Ohm's law and Kirchhoff's law and expressed as

$$E = \frac{V_{\mathrm{PE}}}{b} = \frac{V_2(1 + R_L/R_2) - V_1}{b} \tag{5}$$

where b is the pyroelectric film thickness. Meanwhile, the leakage current is expressed as

$$i_{\mathrm{PE}} = C_1 \frac{\mathrm{d}V_1}{\mathrm{d}t} \tag{6}$$

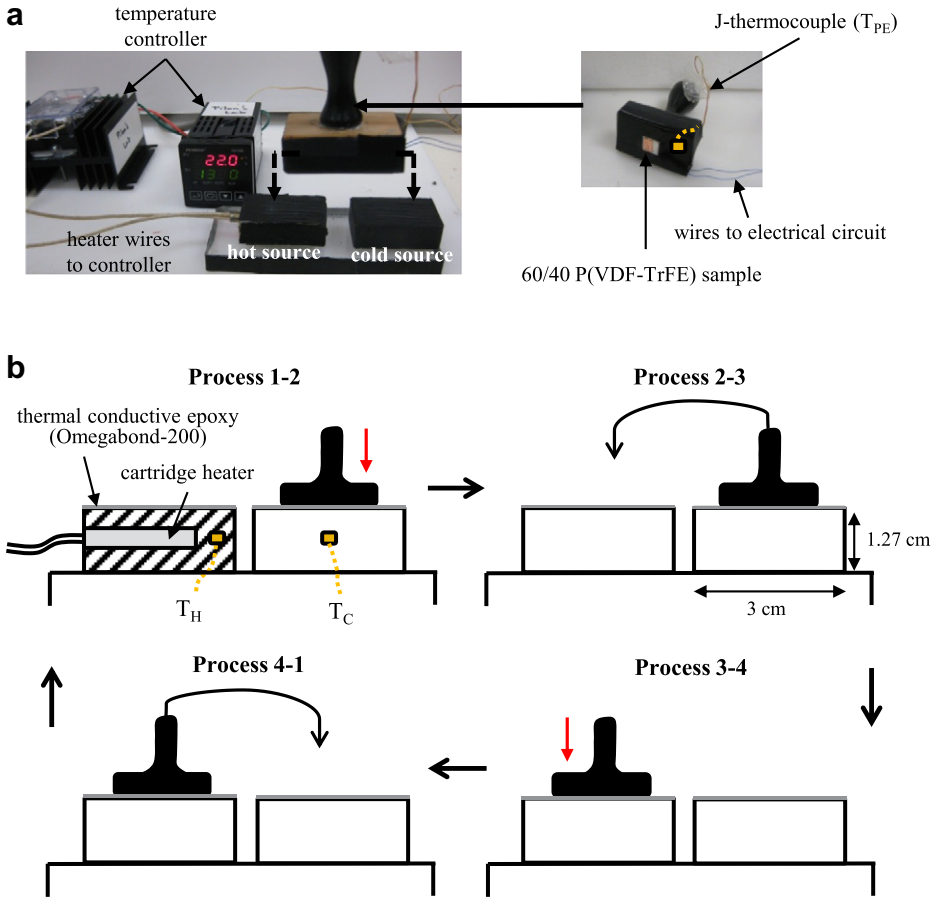

Fig. 2. (a) Thermal subsystem used to create periodic temperature oscillations during the Olsen cycle as well as the PE-stamp assembly (b) Schematic of each process in the Olsen cycle during stamping experiments.

where V_1 is the voltage across the capacitor C_1 as shown in Fig. 3. The same circuit was used to prepole the films. Then, the electrical resistivity of the PE was estimated as

$$\rho_R = \frac{V_{PE}A}{i_{PE}b} \tag{7}$$

3.3. Experimental procedure

First, the P(VDF–TrFE) film was poled under an electric field of 200 kV/cm to increase its electrical resistivity [31]. The temperature of the hot block was set to $T_H = 90$ °C. Then, the stamp assembly supporting the PE was brought in thermal contact with the hot block for 70 min. The PE resistivity was monitored over time until it reached a steady-state. Then, poling was complete and the Olsen cycle was performed.

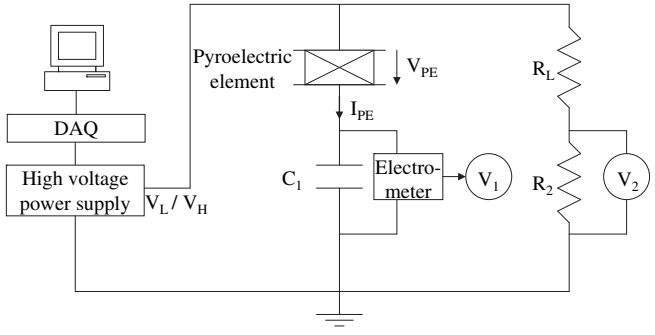

Fig. 3. Electrical circuit used in the present study to prepole and measure the electrical resistivity ρ_R of the pyroelectric element and to perform the Olsen cycle.

To create the time-dependent temperature oscillations required in the Olsen cycle, the PE was successively heated and cooled by manually stamping it against the hot and cold blocks. The time required for the film to reach the temperatures T_H and T_C of the hot and cold reservoirs (Processes 2–3 and 4–1) was greater than that to completely charge or discharge the PE (Processes 1–2 and 3–4). Thus, sufficient time (~8 s) was allowed in Process 4–1 for the sample's electric displacement to reach steady-state ($\partial D/\partial t = 0$). However, due to large leakage current at high temperatures, the sample was placed on the hot block for only ~4 s (Process 2–3) before lowering the electric field (Process 3–4). In other words, Process 2–3 was terminated before the sample had completely discharged and before a steady-state temperature had been reached. Then, the phase transition may have been incomplete.

The epoxy layer, electrically insulating the cold and hot blocks, introduced a thermal contact resistance and reduced heat transfer between the PE and hot or cold blocks. In fact, its thermal conductivity was small compared with that of metals and its surface was uneven. Therefore, pressure was applied between the PE and the hot or cold blocks to try to reduce the thermal contact resistance.

The Olsen cycle was performed for high electric fields E_H ranging from 290 to 475 kV/cm. The low electric field E_L was set as 200 kV/cm to prevent depoling of the film during the cycle [16]. The cold and hot source temperatures were maintained at 25 and 110 °C, respectively, by analogy with the "dipping experiments" reported

in Ref. [16]. In the "dipping experiments", commercial P(VDF–TrFE) films immersed in silicone oil baths could withstand electric fields as high as 600 kV/cm [31]. Unfortunately, in the present "stamping experiments", the film was unable to sustain electric fields larger than 475 kV/cm in air because the dielectric breakdown field of air is lower than that of silicone oil [37].

4. Results and discussion

4.1. Electrical resistivity

Fig. 4 plots the film electrical resistivity ρ_R of the commercial 60/40 P(VDF–TrFE) sample as a function of time during poling at $T_{hot} = 90$ °C and $E = 200$ kV/cm. The film resistivity increased by a factor 4.79 during the first 20 min of poling. After 70 min, it reached 5.22×10^{10} Ω m and did not change noticeably as poling continued. The increase in film resistivity during poling was possibly attributed to the gradual transport of ionic impurities contained within the film to its electrodes [38].

4.2. Temperature oscillations

Fig. 5 shows the temperature of the PE during seven consecutive Olsen cycles at frequencies ranging from 0.066 to 0.078 Hz. The cold source temperature T_C was 25 °C and the hot source temperature T_H was 110 °C. The average minimum and maximum temperatures of the PE during one cycle are denoted by T_{cold} and T_{hot}, respectively. The PE temperature oscillated between $T_{\text{cold}} = 45.2$ °C and $T_{\text{hot}} = 94.8$ °C on average. Note that $T_H > T_{\text{hot}}$ and $T_C < T_{\text{cold}}$ due to the thermal contact resistance between the PE and the hot or cold blocks and the relatively short time they were in thermal contact with each other.

The following subsections report on the effects of several experimental parameters which affect energy density, namely the (i) leakage current, (ii) high electric field E_H, (iii) hot source temperature T_H, and (iv) pressure applied between the aluminum blocks and the PE. The experimental data obtained in this study are summarized in Table 1.

4.3. Effect of leakage current

Fig. 6 plots the D–E diagram obtained for an Olsen cycle performed under electric fields between $E_L \simeq 200$ and $E_H \simeq 350$ kV/cm

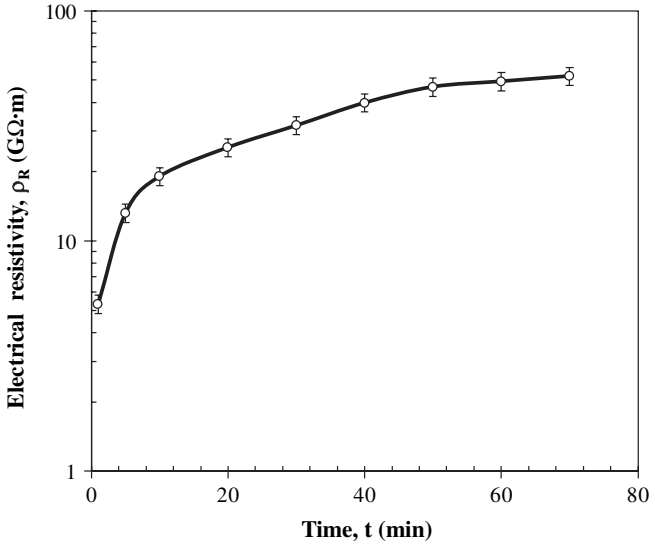

Fig. 4. Electrical resistivity of a 1 cm × 1 cm area and 60.45 μm thick 60/40P(VDF–TrFE) film poled at $E = 200$ kV/cm and $T_{\text{hot}} = 90$ °C as a function of time.

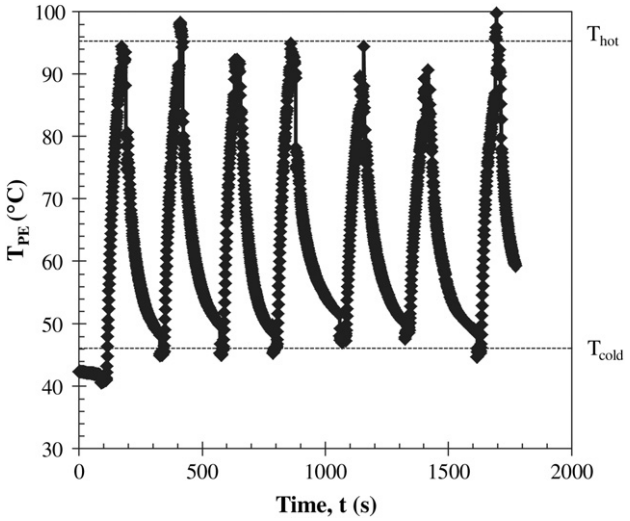

Fig. 5. Temperature of the PE over seven consecutive Olsen cycles. The operating conditions were $T_C = 25$ °C, $T_H = 110$ °C, $E_L = 200$ kV/cm, and $E_H = 350$ kV/cm while the cycle frequency ranged from 0.066 to 0.077 Hz.

and cold and hot sources at $T_C = 25$ °C and $T_H = 110$ °C, respectively. It indicates that the Olsen cycle did not start and end at the same point, as Points 4 and 4′ did not coincide. The offset was caused by leakage current through the PE film [16]. It reduced the electrical energy produced during the Olsen cycles. Indeed, the leakage current increases with increasing temperature and applied electric field [16]. Kouchachvili *et al.* [14] attributed the leakage current to the presence of ionic impurities within the PE film. The current-carrying impurities become mobile and drift towards the electrodes under high temperatures and high electric potentials. Note that Process 3–4 did not follow a smooth path because the phase transition from ferroelectric to paraelectric was incomplete during Process 2–3. Here, an energy density of 155 J/L/cycle was estimated by applying the trapezoidal rule on the 1–2–3–4 region of the D–E curve.

4.4. Effect of hot source temperature T_H

The Curie temperature of 60/40P(VDF–TrFE) was reported to be 66 °C under zero applied electric field [31], 92.5 °C at 300 kV/cm, and 120 °C at 527 kV/cm [10]. When the hot source temperature T_H was set below 110 °C, the temperature T_{hot} reached by the film during the Olsen cycles fell below the Curie temperature when the applied high electric field exceeded 350 kV/cm. As a consequence, a complete ferroelectric to paraelectric transition was not observed for $E_H > 350$ kV/cm. However, when the hot source temperature was increased from 110 °C to 130 °C to further increase T_{hot},

Table 1
List of operating conditions and results obtained in the stamping experiments. The imposed conditions were $E_L = 200$ kV/cm, $T_C = 25$ °C, $T_H = 110$ °C.

E_H	N_D	P_D	ΔT_{PE}	T_{cold}	T_{hot}	f
kV/cm	J/L/cycle	W/L	°C	°C	°C	Hz
290	77.8	4.99	33.9	52.2	86.1	0.064
300	101	6.03	56.3	42.7	99.0	0.060
320	145	10.80	41.2	50.4	91.6	0.075
330	148	9.02	49.7	47.0	96.7	0.061
350	**155**	10.3	55.1	46.8	99.7	0.066
350	146	**11.2**	49.6	44.8	99.4	0.077
350	154	10.5	48.2	49.3	97.5	0.068
350	143	10.4	46.4	48.0	94.4	0.073
350	115	8.90	41.7	47.5	89.2	0.077
379	150	9.72	37.5	55.0	92.5	0.064
475	72.6	5.38	56.3	40.7	97.0	0.074

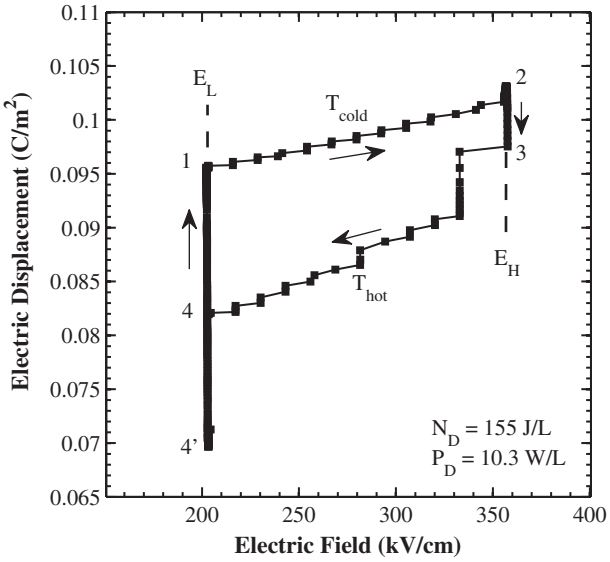

Fig. 6. Experimental Olsen cycle in the electric displacement versus electric field (D–E) diagram obtained with a 1 cm × 1 cm area and 60.45 μm thick 60/40P(VDF–TrFE) film, between T_C = 25 °C and T_H = 110 °C with E_L = 200 kV/cm and E_H = 350 kV/cm.

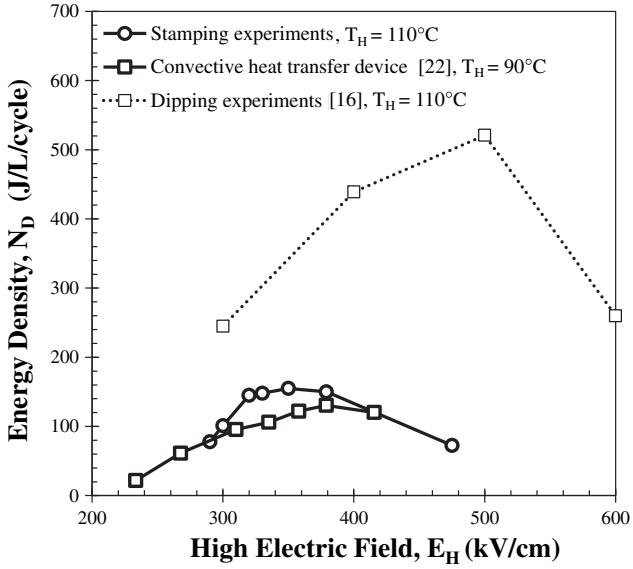

Fig. 7. Comparison of energy density N_D as a function of high electric field E_H obtained in the present study with previously reported experiments. Operating conditions were (1) E_L = 200 kV/cm, E_H = 290–475 kV/cm, T_C = 25 °C (present study), (2) E_L = 200 kV/cm, E_H = 300–600 kV/cm, T_C = 25 °C (dipping experiments) [16], and (3) E_L = 202 kV/cm, E_H = 233–475 kV/cm, T_C = 25 °C (convective heat transfer device) [22].

electrical sparks were observed during the Olsen cycles. We speculate that the short-circuit was attributed to the reduction in the dielectric strength of air near the hot block with increasing temperatures [37]. In addition, increasing the hot source temperature beyond 110 °C resulted in excessive leakage current. Under these conditions, the rate of surface charges conducting through the film exceeded the rate of electrical discharge during Process 2–3 over time. This resulted in crossovers in the D-E curves between Processes 1–2 and 3–4. Therefore, the hot source temperature T_H of 110 °C was found to be optimum to maximize energy density for 60/40P(VDF–TrFE).

4.5. Effect of high electric field E_H

Fig. 7 shows the energy density produced in the stamping experiments as a function of applied high electric field E_H spanning from 290 to 475 kV/cm. The cold and hot source temperatures were 25 °C and 110 °C, respectively. The low electric field E_L was set as 200 kV/cm and the cycles operated at frequencies between 0.060 and 0.077 Hz. The range of high electric field E_H was selected by analogy with our previous pyroelectric energy generation experiments using 60/40P(VDF–TrFE) [16,22]. Fig. 7 indicates that the energy density increased with increasing E_H up to 350 kV/cm before decreasing for higher electric field. The largest amount of energy generated was 155 J/L/cycle for E_H = 350 kV/cm at 0.066 Hz, corresponding to a power density of 10.3 W/L. The associated cycle was shown in Fig. 6. This can be explained by the fact that as the high electric field E_H increased, the electric field span ($E_H - E_L$) increased, resulting in large energy and power densities produced during the Olsen cycle according to Equations (2) and (3). However, leakage current was also found to increase with increasing electric field. Overall, increasing E_H beyond 350 kV/cm resulted in a reduction in the generated energy density.

4.6. Effect of applied pressure

The thermal contact resistance between the PE and aluminum blocks can be reduced by increasing the pressure applied to the film [39]. In turn, this could reduce the time necessary for the sample to reach the cold and hot source temperatures thus, increasing the power density. The pressure applied to the PE throughout the Olsen cycle varied from 0 to ~200 kPa. However, application of excessive pressure (>200 kPa) caused electrical short-circuits in the PE when in contact with the hot block. This could be attributed to the development of microcracks between the electrodes when pressed against the uneven aluminum blocks. No significant effects on the heating and cooling times were observed for applied pressures smaller than 200 kPa.

4.7. Discussion

The Olsen cycle requires the application of high electric fields across the pyroelectric material. The corresponding voltages can be prohibitively large for implementation in devices. However, the use of very thin film would substantially reduce the voltage required. Then, the Olsen cycle may be performed by using several batteries connected in series. Leakage current however may increase with decreasing film thickness [40,41].

4.8. Comparison with other heat transfer modes

Fig. 7 compares the energy density obtained for 60/40P(VDF–TrFE) as a function of high electric field E_H in the present study with results reported for "dipping experiments" [16] and the pyroelectric converter constructed by Nguyen *et al.* [22]. It indicates that the heat transfer mechanism used to generate temperature oscillations played an important role in the amount of pyroelectric energy generated. Fig. 7 also establishes that the largest energy density generated in the "stamping experiments" (155 J/L/cycle) exceeded the 130 J/L/cycle obtained with the device reported in Ref. [22] for similar operating conditions, T_{hot} = 83 °C and E_H = 223.7–415.6 kV/cm. However, it was significantly smaller than the energy densities obtained in "dipping experiments" [16]. This can be attributed to the higher PE temperatures (T_{hot} = 100 °C) and higher applied electric fields (E_H = 600 kV/cm) imposed in the "dipping experiments" [16] compared with T_{hot} = 87–96 °C and

Table 2
Comparison of maximum power density achieved using either the Olsen cycle or the pyroelectric effect for different materials, temperature ranges, and frequencies.

Material	Technique	T_{cold}	T_{hot}	f	P_D	Ref.
–	–	°C	°C	Hz	W/L	–
PZST	Olsen cycle	156.8	177.4	0.26	33.9	[11]
73/27P(VDF–TrFE)	Olsen cycle	23.0	67.0	0.079	2.38	[33]
60/40P(VDF–TrFE)	Olsen cycle	58.3	76.5	0.256	13.3	[13]
60/40P(VDF–TrFE)	Olsen cycle	67.3	81.4	0.12	10.7	[22]
60/40P(VDF–TrFE)	Olsen cycle	25.0	110.0	0.10	52.1	[16]
PZN-4.5PT	Olsen cycle	100.0	160.0	0.10	24.3	[19]
PZN-5.5PT	Olsen cycle	100.0	190.0	0.10	11.7	[35]
PMN-32PT	Olsen cycle	80.0	170.0	0.049	4.92	[27]
PZT	Pyroelectric effect	80.0	110.0	5.0	1.2×10^{-3}	[43]
PZT	Pyroelectric effect	31.0	62.0	0.00875	1.6×10^{-3}	[23]
PZT	Pyroelectric effect	14.0	93.5	0.42	0.15	[26,44]
$LiTaO_3$	Pyroelectric effect	27.0	37.0	0.01	5.21×10^{-2}	[45]
PMN-30PT	Pyroelectric effect	32.0	40.4	0.10	8.64×10^{-3}	[24]
PMN-25PT	Pyroelectric effect	N/A	N/A	1.0	3.76	[46]

E_H = 290–475 kV/cm in the "stamping experiments". This was made possible by the use of silicone oil which has a larger electric breakdown field strength than air [37].

Finally, Table 1 indicates that the maximum values of power density and energy density did not correspond to the same operating frequency. In addition, the peak power density of 11.2 W/L at 0.077 Hz observed in the present study was a slight improvement over the 10.7 W/L at 0.12 Hz reported by Nguyen *et al.* [22]. However, the present procedure is significantly simpler to implement.

4.9. Comparison with other pyroelectric energy harvesting methods

Attempts have been made to use the pyroelectric effect to produce electricity from temperature oscillations but without using the Olsen cycle. Unfortunately, this approach resulted in relatively small power density regardless of the heating and cooling methods considered as predicted by van der Ziel [42]. Cuadras *et al.* [23] blew periodic pulses of hot and cold air to create temperature oscillations in PZT and PVDF samples. They achieved a power density of 0.0016 W/L at 0.0088 Hz with 100 μm thick PZT for temperatures between 31 and 62 °C. Mane *et al.* [24] used infrared radiation for heating and natural convection for cooling lead zirconate titanate (PZT), pre-stressed PZT composite, and single crystal PMN-30PT samples. The maximum power density achieved was 0.00864 W/L with 270 μm thick PMN-30PT at frequency 0.1 Hz corresponding to a temperature swing of about 8.4 °C. Similar experiments using radiative heating were performed by Buchanan *et al.* [43] on 1 μm thick PZT 90/10 samples. They obtained about 0.0012 W/L at 5 Hz between 80 and 110 °C. Ravindran *et al.* [26,44] operated a pyroelectric generator that utilizes the pressure expansion of air to move heat from a heat source to 200 μm PZT attached to a heat sink. The authors reported a power density of 0.15 W/L at 0.42 Hz for a temperature difference of 79.5 K. Chang *et al.* [45] built a pyroelectric energy harvesting device that utilizes shape memory alloy springs to oscillate a $LaTiO_3$ sample in thermal contact between a hot and a cold reservoir maintained at 310 and 300 K, respectively. The maximum power produced was 0.0521 W/L at 0.01 Hz. Finally, Sebald *et al.* [46] generated a 2 °C temperature variation across 850 μm thick single crystal PMN-25PT and harvested 3.76 W/L at 1 Hz.

The above results should be compared with those achieved by performing the Olsen cycle. In fact, Table 2 compares the maximum power density achieved using either the Olsen cycle or the pyroelectric effect for different materials, temperature ranges, and frequencies. In particular, Olsen *et al.* [11] obtained 33.9 W/L in a device at 0.26 Hz between 150 and 180 °C using PZST. Nguyen *et al.* [22] achieved 10.7 W/L in a device similar to that of Olsen *et al.* [11] but operating at 0.12 Hz between 67.3 and 81.4 °C using 60/40 P(VDF–TrFE). Ikura [13] reported a maximum power density of 13.3 W/L for 60/40P(VDF–TrFE) subjected to dipping experiments at 0.256 Hz between 58 and 76 °C. Similarly, Navid *et al.* [16] reported 52.1 W/L for 60/40P(VDF–TrFE) dipping experiments at 0.10 Hz between 25 and 110 °C. In the present study, we have achieved 11.2 W/L at 0.077 Hz between 44.8 and 99.4 °C using 60/40P(VDF–TrFE) and a new stamping technique. Other results for single crystal PMN-32PT [27] and PZN-5.5PT [35] are also reported in Table 2. Overall, performing the Olsen cycle enables one to generate significantly more power than by simply using the pyroelectric effect.

5. Conclusion

This paper reported experimental measurements of the energy and power densities generated by subjecting 60/40P(VDF–TrFE) films to the Olsen cycle. Heating and cooling of the film were achieved by conductive heat transfer using a stamping technique. Results were compared with data collected from a device using laminar forced convective heat transfer [22] and from dipping experiments [16]. The largest energy density generated by 60/40P(VDF–TrFE) in this study was 155 J/L/cycle at 0.066 Hz with cold and hot temperatures of 25 and 110 °C, respectively, and electric field cycled between 200 and 350 kV/cm. These operating conditions represent a tradeoff between maximizing applied high electric field E_H and hot source temperature $T_{H,}$ on the one hand, and minimizing leakage current on the other. Moreover, the energy and power densities obtained in the current study were larger than those achieved by the device assembled by Nguyen *et al.* [22]. Finally, the proposed stamping procedure can be implemented in a compact automated device.

Acknowledgements

F.Y. Lee is indebted to the UCLA Mechanical and Aerospace Engineering Department for financial support in the form of a Graduate Fellowship.

References

[1] Lawrence Livermore National Laboratory, U.S. Energy Flow Trends – 2009 (September 16, 2011).https://publicaffairs.llnl.gov/news/energy/energy.html#2009.
[2] L. Kouchachvili, M. Ikura, Pyroelectric conversion – effects of P(VDF–TrFE) preconditioning on power conversion, Journal of Electrostatics 65 (1) (2006) 182–188.

[3] D.G. Thombare, S.K. Verma, Technological development in the Stirling cycle engines, Renewable and Sustainable Energy Reviews 12 (2008) 1–38.
[4] B.T. Liu, K.H. Chien, C.C. Wang, Effect of working fluids on organic Rankine cycle for waste heat recovery, Energy 29 (8) (2004) 1207–1217.
[5] L. Kouchachvili, M. Ikura, Improving the efficiency of pyroelectric conversion, International Journal of Energy Research 32 (2008) 328–335.
[6] S.B. Riffat, X. Ma, Thermoelectrics: a review of present and potential applications, Applied Thermal Engineering 23 (8) (2003) 913–935.
[7] R.B. Olsen, D.A. Bruno, J.M. Briscoe, W.F. Butler, A pyroelectric energy converter which employs regeneration, Ferroelectrics 38 (1–4) (1981) 975–978.
[8] R.B. Olsen, Ferroelectric conversion of heat to electrical energy – a demonstration, Journal of Energy 6 (1982) 91–95.
[9] R.B. Olsen, D.D. Brown, High-efficiency direct conversion of heat to electrical energy related pyroelectric measurements, Ferroelectrics 40 (1–2) (1982) 17–27.
[10] R.B. Olsen, D.A. Bruno, Pyroelectric Conversion Materials, Proceedings of the 21st Intersociety Energy Conversion Engineering Conference, American Chemical Society, San Diego, CA, August 25–29, 1986, 89–93.
[11] R.B. Olsen, D.A. Bruno, J.M. Briscoe, Cascaded pyroelectric energy converter, Ferroelectrics 59 (3–4) (1984) 205–219.
[12] R.B. Olsen, D.A. Bruno, J.M. Briscoe, Pyroelectric conversion cycles, Journal of Applied Physics 58 (12) (1985) 4709–4716.
[13] M. Ikura, Conversion of low-grade heat to electricity using pyroelectric copolymer, Ferroelectrics 267 (2002) 403–408.
[14] L. Kouchachvili and M. Ikura, High performance P(VDF-TrFE) copolymer for pyroelectric conversion, U.S. Patent, no. 7,323,506, 2006.
[15] A. Navid, D. Vanderpool, A. Bah, L. Pilon, Towards optimization of a pyroelectric energy converter for harvesting waste heat, International Journal of Heat and Mass Transfer 53 (19–20) (2010) 4060–4070.
[16] A. Navid, L. Pilon, Pyroelectric energy harvesting using Olsen cycles in purified and porous poly(vinylidene fluoride–trifuoroethylene) thin films, Smart Materials and Structures 20 (2) (2011) 025012.
[17] G. Sebald, L. Seveyrat, D. Guyomar, L. Lebrun, B. Guiffard, S. Pruvost, Electrocaloric and pyroelectric properties of 0.75Pb(Mg 1/3 Nb 2/3)O_3–0.25$PbTiO_3$ single crystals, Journal of Applied Physics 100 (124112) (2006) 1–6.
[18] D. Guyomar, S. Pruvost, G. Sebald, Energy harvesting based on FE–FE transition in ferroelectric single crystals, IEEE Transactions on Ultrasonics, Ferroelectrics, and Frequency Control 55 (2008) 279–285.
[19] A. Khodayari, S. Pruvost, G. Sebald, D. Guyomar, S. Mohammadi, Nonlinear pyroelectric energy harvesting from relaxor single crystals, IEEE Transactions on Ultrasonics, Ferroelectrics, and Frequency Control 56 (2009) 693–699.
[20] H. Zhu, S. Pruvost, D. Guyomar, A. Khodayari, Thermal energy harvesting from $Pb(Zn_{1/3}Nb_{2/3})_{0.955}Ti_{0.045}O_3$ single crystals phase transitions, Journal of Applied Physics 106 (12) (2009) 124102.
[21] J. Fang, H. Frederich, L. Pilon, Harvesting nanoscale thermal radiation using pyroelectric materials, ASME Journal of Heat Transfer 132 (9) (2010) 092701.
[22] H. Nguyen, A. Navid, L. Pilon, Pyroelectric energy converter using co-polymer P(VDF–TrFE) and the Olsen cycle cycle for waste heat energy harvesting, Applied Thermal Engineering 30 (2010) 2127–2137.
[23] M. Cuadras, V. Gasulla Ferrari, Thermal energy harvesting through pyroelectricity, Sensors and Actuators A: Physical 158 (1) (2010) 132–139.
[24] P. Mane, J. Xie, K. Leang, K. Mossi, Cyclic energy harvesting from pyroelectric materials, IEEE Transactions on Ultrasonics, Ferroelectrics, and Frequency Control 58 (1) (2011) 10–17.
[25] S. Hunter, N. Lavrik, T. Bannuru, S. Mostafa, S. Rajic, P. Datskos, Development of MEMS based pyroelectric thermal energy harvesters Orlando, FL, in: N. Dhar, P. Wijewarnasuriya, A. Dutta (Eds.), Energy Harvesting and Storage: Materials, Devices, and Applications II (April 25, 2011), p. 80350.
[26] S.K.T. Ravindran, T. Huesgen, M. Kroener, P. Woias, A Self-Sustaining Pyroelectric Energy Harvester Utilizing Spatial Thermal Gradients, in Solid-State Sensors, Actuators and Microsystems Conference (TRANSDUCERS), 2011 16th International, Beijing, China, June 5–9 2011, 657–660.
[27] R. Kandilian, A. Navid, L. Pilon, The pyroelectric energy harvesting capabilities of PMN-PT near the morphotropic phase boundary, Smart Material and Structures 20 (1) (2011) 055020.
[28] S.B. Lang, Sourcebook of Pyroelectricity, Gordon and Breach, Science Publishers, Inc., New York, NY, 1974.
[29] S.B. Lang, D.K. Das-Gupta, Handbook of Advanced Electronic and Photonic Materials and Devices, vol. 4, Academic Press, San Diego, CA, 2001.
[30] M.E. Lines, A.M. Glass, Principles and Applications of Ferroelectrics and Related Materials, Clarendon Press, Oxford, UK, 1977.
[31] A. Navid, C.S. Lynch, L. Pilon, Purified and porous poly(vinylidene fluoride–trifluoroethylene) [P(VDF–TrFE)] thin films for pyroelectric infrared sensing and energy harvesting, Smart Materials and Structures 19 (2010) 055006.
[32] H. Yamazaki, J. Ohwaki, T. Yamada, T. Kitayama, Temperature dependence of the pyroelectric response of vinylidene fluoride trifluoroethylene copolymer and the effect of its poling conditions, Applied Physics Letters 39 (1981) 772–773.
[33] R.B. Olsen, D.A. Bruno, J.M. Briscoe, Pyroelectric conversion cycle of vinylidene fluoride–trifluoroethylene copolymer, Journal of Applied Physics 57 (11) (1985) 5036–5042.
[34] J. Yu, M. Ikura, Direct Conversion of Low-grade Heat to Electricity Using Pyrorelectric Conversion, Proceedings of the Fourth IASTED International Conference European Power and Energy Systems, Rhodes, Greece, 2004, 442–446.
[35] I. McKinley, R. Kandilian, and L. Pilon, Waste heat energy harvesting using Olsen cycle on 0.945$Pb(Zn_{1/3}\ Nb_{2/3})O_3-0.055PbTiO_3$ single crystals, Smart Material and Structures (accepted).
[36] Omega Engineering, Thermally Conductive Epoxies and Thermally Conductive Grease (June 14, 2011).http://www.omega.com/pptst/OB100_OB200_OT200.html.
[37] E.O. Forster, H. Yamashita, C. Mazzetti, C. Pompili, L. Caroli, S. Patrissi, The effect of electrode gap on breakdown in liquid dielectrics, IEEE Transactions on Dielectrics and Electical Insulation 1 (3) (1994) 440–446.
[38] L. Kouchachvili and M. Ikura, High performance P(VDF-TrFE) copolymer for pyroelectric conversion, US Patent No. 7,323,506, January 29, 2008.
[39] F.P. Incropera, D.P. DeWitt, T. Bergman, A. Lavine, Fundamentals of Heat and Mass Transfer, John Wiley and Sons, Ltd., New York, NY, 2006.
[40] F.Y. Chen, Y.K. Fang, C.Y. Hsu, J.R. Chen, Time response analysis of a pyroelectric detector, Ferroelectrics 200 (1) (1997) 257–268.
[41] M.C. Kao, C.M. Wang, H.Z. Chen, M.S. Lee, Y.C. Chen, Thickness-dependent leakage current of (polyvinylidene fluoride/lead titanate) pyroelectric detectors, IEEE Transactions on Ultrasonics, Ferroelectrics, and Frequency Control 50 (8) (2003) 958–964.
[42] A. van der Ziel, Solar power generation with the pyroelectric effect, Journal of Applied Physics 45 (9) (1974) 4128.
[43] R. Buchanan, J. Huang, Pyroelectric and sensor properties of ferroelectric thin films for energy conversion, Journal of the European Ceramic Society 98 (1999) 1467–1471.
[44] S.K.T. Ravindran, T. Huesgen, M. Kroener, P. Woias, A self-sustaining micro thermomechanic pyroelectric generator, Applied Physics Letters 99 (2011) 104102.
[45] H.H.S. Chang, Z. Huang, Laminate composites with enhanced pyroelectric effects for energy harvesting, Smart Materials and Structures 19 (1) (2010) 065018.
[46] G. Sebald, E. Lefeuvre, D. Guyomar, Pyroelectric energy conversion: optimization principles, IEEE Transactions on Ultrasonics, Ferroelectrics, and Frequency Control 55 (2008) 538–551.